



Global Analyses of Neutrino Oscillation Experiments

M.C. Gonzalez-Garcia^{a,b}, Michele Maltoni^c, Thomas Schwetz^d

^a*Institució Catalana de Recerca i Estudis Avançats (ICREA), Departament d'Estructura i Constituents de la Matèria and Institut de Ciències del Cosmos, Universitat de Barcelona, Diagonal 647, E-08028 Barcelona, Spain*

^b*C.N. Yang Institute for Theoretical Physics, State University of New York at Stony Brook, Stony Brook, NY 11794-3840, USA*

^c*Instituto de Física Teórica UAM/CSIC, Calle de Nicolás Cabrera 13–15, Universidad Autónoma de Madrid, Cantoblanco, E-28049 Madrid, Spain*

^d*Institut für Kernphysik, Karlsruher Institut für Technologie (KIT), D-76021 Karlsruhe, Germany*

Abstract

We summarize the determination of some neutrino properties from the global analysis of solar, atmospheric, reactor, and accelerator neutrino data in the framework of three-neutrino mixing as well as in some extended scenarios such as the mixing with eV-scale sterile neutrinos invoked for the interpretation of the short baseline anomalies, and the presence of non-standard neutrino interactions.

1. Introduction: the New Minimal Standard Model

Thanks to remarkable discoveries by a number of neutrino oscillation experiments it is now an established fact that neutrinos have mass and leptonic flavors are not symmetries of Nature [1, 2]. Historically neutrino oscillations were first observed in the disappearance of solar ν_e 's and atmospheric ν_μ 's which could be interpreted as flavor oscillations with two very different wavelengths. Over the last 15 years, these effects were confirmed also with terrestrial experiments using man made beams from accelerators and nuclear reactors (see Ref. [3] for an overview). In brief, at present we have observed neutrino oscillation effects in:

- atmospheric neutrinos, in particular in the high-statistics results of Super-Kamiokande [4];
- event rates of solar neutrino radiochemical experiments Chlorine [5], Gallex/GNO [6] and SAGE [7], as well as time and energy dependent rates from the four phases in Super-Kamiokande [8–11], the three phases of SNO [12], and Borexino [13, 14];
- disappearance results from accelerator long baseline (LBL) experiments in the form of the energy distribution of ν_μ and $\bar{\nu}_\mu$ events in MINOS [15] and T2K [16], and ν_μ events in NO ν A [17];
- LBL ν_e appearance results for both neutrino and antineutrino events in MINOS [18], and ν_e appearance in NO ν A [17] and T2K [19];

Email addresses: maria.gonzalez-garcia@stonybrook.edu (M.C. Gonzalez-Garcia), michele.maltoni@csic.es (Michele Maltoni), schwetz@kit.edu (Thomas Schwetz)

- reactor $\bar{\nu}_e$ disappearance at medium baselines in the form of the energy distribution of events in Double Chooz [20], Daya Bay [21] and RENO [22];
- the energy spectrum of reactor $\bar{\nu}_e$ disappearance at LBL in KamLAND [23].

These results imply that *neutrinos are massive* and *there is physics beyond the Standard Model (SM)*. The fundamental question arises, what is the underlying theory for neutrino masses. In this article, however, we will focus on the more mundane but difficult approach of the detailed determination of the simplest low energy parametrization(s) required to describe the bulk of data.

The SM is a gauge theory based on the gauge symmetry $SU(3)_C \times SU(2)_L \times U(1)_Y$ spontaneously broken to $SU(3)_C \times U(1)_{EM}$ by the the vacuum expectation value of a Higgs doublet field ϕ . The SM contains three fermion generations which reside in chiral representations of the gauge group. Right-handed fields are included for charged fermions as they are needed to build the electromagnetic and strong currents. However, no right-handed neutrinos are included in the model since neutrinos are neutral and colourless and therefore the right-handed neutrinos are singlets of the SM group.

In the SM, fermion masses arise from the Yukawa interactions which couple the right-handed fermion singlets to the left-handed fermion doublets and the Higgs doublet. After spontaneous electroweak symmetry breaking these interactions lead to charged fermion masses but leave the neutrinos massless. No Yukawa interaction can be written that would give a tree level mass to the neutrino because no right-handed neutrino field exists in the model.

Furthermore, within the SM $G_{SM}^{\text{global}} = U(1)_B \times U(1)_e \times U(1)_\mu \times U(1)_\tau$ is an accidental global symmetry. Here $U(1)_B$ is the baryon number symmetry, and $U(1)_{e,\mu,\tau}$ are the three lepton flavor symmetries. Any neutrino mass term which could be built with the particle content of the SM would violate the $U(1)_L$ subgroup of G_{SM}^{global} and therefore cannot be induced by loop corrections. Also, it cannot be induced by non-perturbative corrections because the $U(1)_{B-L}$ subgroup of G_{SM}^{global} is non-anomalous.

It follows then that the SM predicts that neutrinos are *strictly* massless. Consequently, there is neither mixing nor CP violation in the leptonic sector. Clearly this is in contradiction with the neutrino data summarized above. So the Standard Model has to be extended at least to include neutrino masses. This minimal extension is what we call the *New Minimal Standard Model (NMSM)*.

The two minimal extensions to give neutrino mass and explain the data are:

- to introduce ν_R and impose total lepton number (L) conservation. After spontaneous electroweak symmetry breaking we have:

$$\mathcal{L}_D = \mathcal{L}_{SM} - M_\nu \bar{\nu}_L \nu_R + \text{h.c.} \quad (1)$$

In this case mass eigenstate neutrinos are Dirac fermions, *i.e.*, $\nu^c \neq \nu$;

- to construct a mass term only with the SM left-handed neutrinos by allowing L violation:

$$\mathcal{L}_M = \mathcal{L}_{SM} - \frac{1}{2} M_\nu \bar{\nu}_L \nu_L^c + \text{h.c.} \quad (2)$$

In this case the mass eigenstates are Majorana fermions, $\nu^c = \nu$. Note that the Majorana mass term above breaks the electroweak gauge invariance, and therefore spoils the renormalizability of the model. In this respect \mathcal{L}_M can only be understood as a low energy limit of a complete theory, whereas \mathcal{L}_D is formally self-consistent.

Either way, in the NMSM flavour is mixed in the CC interactions of the leptons, and a leptonic mixing matrix appears analogous to the CKM matrix for the quarks. However the discussion of leptonic mixing is complicated by two factors. First the number massive neutrinos (n) is unknown, since there are no constraints on the number of right-handed (SM-singlet) neutrinos. Second, since neutrinos carry neither color nor electromagnetic charge, they could be Majorana fermions. As a consequence the number of new parameters in the model depends on the number of massive neutrino states and on whether they are Dirac or Majorana particles.

In general, if we denote the neutrino mass eigenstates by ν_i , $i = 1, 2, \dots, n$, and the charged lepton mass eigenstates by $l_i = (e, \mu, \tau)$, in the mass basis, leptonic CC interactions are given by

$$-\mathcal{L}_{CC} = \frac{g}{\sqrt{2}} \bar{l}_{iL} \gamma^\mu U^{ij} \nu_j W_\mu^+ + \text{h.c.} \quad (3)$$

Here U is a $3 \times n$ matrix which verifies $UU^\dagger = I_{3 \times 3}$ but in general $U^\dagger U \neq I_{n \times n}$. This is the case, for example, when considering mixing with non-doublet states, such as discussed in Sec. 4.

In what follows we will review the status of the analysis of the oscillation neutrino data in different frameworks. In Sec. 2 we present the results for the case of three-neutrino mixing, and in Sec. 3 we discuss the implications of such results for observables sensitive to the absolute neutrino mass scale. In Sec. 4 we focus on extended scenarios involving mixing with eV-scale sterile neutrinos, as invoked for the interpretation of the short baseline anomalies. In Sec. 5 we derive limits on the presence of non-standard neutrino-matter interactions.

2. Analysis in the framework of three-neutrino mixing

The wealth of data listed in the introduction can be consistently described by assuming mixing among the three known neutrinos (ν_e, ν_μ, ν_τ), which can be expressed as quantum superpositions of three massive states ν_i ($i = 1, 2, 3$) with masses m_i . As explained in the previous section this implies the presence of a leptonic mixing matrix in the weak charged current interactions which can be parametrized as [24]:

$$U = \begin{pmatrix} c_{12}c_{13} & s_{12}c_{13} & s_{13}e^{-i\delta_{CP}} \\ -s_{12}c_{23} - c_{12}s_{13}s_{23}e^{i\delta_{CP}} & c_{12}c_{23} - s_{12}s_{13}s_{23}e^{i\delta_{CP}} & c_{13}s_{23} \\ s_{12}s_{23} - c_{12}s_{13}c_{23}e^{i\delta_{CP}} & -c_{12}s_{23} - s_{12}s_{13}c_{23}e^{i\delta_{CP}} & c_{13}c_{23} \end{pmatrix} \begin{pmatrix} e^{i\alpha_1} & 0 & 0 \\ 0 & e^{i\alpha_2} & 0 \\ 0 & 0 & 1 \end{pmatrix} \quad (4)$$

where $c_{ij} \equiv \cos \theta_{ij}$ and $s_{ij} \equiv \sin \theta_{ij}$. In addition to the Dirac-type phase δ_{CP} , analogous to that of the quark sector, there are two extra phases α_1, α_2 associated to a possible Majorana character of neutrinos. Such phases, however, are not relevant for neutrino oscillations.

In this convention, disappearance of solar ν_e 's and long baseline reactor $\bar{\nu}_e$'s proceeds dominantly via oscillations with wavelength $\propto E/\Delta m_{21}^2$ ($\Delta m_{ij}^2 \equiv m_i^2 - m_j^2$ and $\Delta m_{21}^2 \geq 0$ by convention) and amplitudes controlled by θ_{12} , while disappearance of atmospheric and LBL accelerator ν_μ 's proceeds dominantly via oscillations with wavelength $\propto E/|\Delta m_{31}^2| \ll E/\Delta m_{21}^2$ and amplitudes controlled by θ_{23} . The angle θ_{13} controls the amplitude of oscillations involving ν_e flavor with $E/|\Delta m_{31}^2|$ wavelengths. Given the observed hierarchy between the solar and atmospheric wavelengths there are two possible non-equivalent orderings for the mass eigenvalues, which are conventionally chosen as

$$\Delta m_{21}^2 \ll (\Delta m_{32}^2 \simeq \Delta m_{31}^2 > 0); \quad (5)$$

$$\Delta m_{21}^2 \ll -(\Delta m_{31}^2 \simeq \Delta m_{32}^2 < 0), \quad (6)$$

As it is customary we refer to the first option, Eq. (5), as Normal Ordering (NO), and to the second one, Eq. (6), as Inverted Ordering (IO); in this form they correspond to the two possible choices of the sign of Δm_{31}^2 . In this convention the angles θ_{ij} can be taken without loss of generality to lie in the first quadrant, $\theta_{ij} \in [0, \pi/2]$, and the CP phase $\delta_{CP} \in [0, 2\pi]$. In the following we adopt the (arbitrary) convention of reporting results for Δm_{31}^2 for NO and Δm_{32}^2 for IO, *i.e.*, we always use the one which has the larger absolute value. Sometimes we will generically denote such quantity as $\Delta m_{3\ell}^2$, with $\ell = 1$ for NO and $\ell = 2$ for IO.

In summary, the 3ν oscillation analysis of the existing data involves six parameters: 2 mass differences (one of which can be positive or negative), 3 mixing angles, and the CP phase δ_{CP} . For the sake of clarity we summarize in Table 1 which experiment contribute dominantly to the present determination of the different parameters.

The consistent determination of these leptonic parameters requires a global analysis of the data described above. Such global fits are presently performed by a few phenomenological groups [25–27]; here we summarize the results from Ref. [27, 28]. We show in Fig. 1 the one-dimensional projections of the $\Delta\chi^2$ of the

Experiment	Dominant	Important
Solar Experiments	θ_{12}	$\Delta m_{21}^2, \theta_{13}$
Reactor LBL (KamLAND)	Δm_{21}^2	θ_{12}, θ_{13}
Reactor MBL (Daya-Bay, Reno, D-Chooz)	θ_{13}	$ \Delta m_{3\ell}^2 $
Atmospheric Experiments	θ_{23}	$ \Delta m_{3\ell}^2 , \theta_{13}, \delta_{\text{CP}}$
Accelerator LBL ν_{μ} Disapp (Minos, NOvA, T2K)	$ \Delta m_{3\ell}^2 , \theta_{23}$	
Accelerator LBL ν_e App (Minos, NOvA, T2K)	δ_{CP}	$\theta_{13}, \theta_{23}, \text{sign}(\Delta m_{3\ell}^2)$

Table 1. Experiments contributing to the present determination of the oscillation parameters.

global analysis as a function of each of the six parameters. The corresponding best fit values and the derived ranges for the six parameters at the 1σ (3σ) level are given in Tab. 2. For each parameter the curves and ranges are obtained after marginalizing with respect to the other five parameters. The results in the table are shown for three scenarios. In the first and second columns we assume that the ordering of the neutrino mass states is known “a priori” to be Normal or Inverted, respectively, so the ranges of all parameters are defined with respect to the minimum in the given scenario. In the third column we make no assumptions on the ordering, so in this case the parameter ranges are defined with respect to the global minimum (which corresponds to Inverted Ordering) and are obtained marginalizing also over the ordering. For this third case we only give the 3σ intervals. Of course in this case the range of $\Delta m_{3\ell}^2$ is composed of two disconnected intervals, one one containing the absolute minimum (IO) and the other the secondary local minimum (NO).

As already mentioned, all the data described above can be consistently interpreted as oscillations of the three known active neutrinos. In addition to these data, however, several anomalies at short baselines (SBL) have been observed which cannot be explained as 3ν oscillations, but could be interpreted as oscillations involving an $O(\text{eV})$ mass sterile state. They will be discussed in detail in Sec. 4. For what concerns the analysis presented here the only SBL effect which has to be taken into account is the so called *reactor anomaly*. It turns out that the most recent reactor flux calculations [29, 30] fall short at describing the results from reactor experiments at baselines $\lesssim 100$ m, such as Bugey4 [31], ROVNO4 [32], Bugey3 [33], Krasnoyarsk [34, 35], ILL [36], Gösgen [37], SRP [38], and ROVNO88 [39]. Such reactor short-baseline experiments (RSBL) do not contribute to oscillation physics in the 3ν framework, but they play an important role in constraining the unoscillated reactor neutrino flux if they are used instead of the theoretically calculated reactor fluxes. Thus to account for the possible effect of the reactor anomaly in the determined ranges of neutrino parameters we show the results in Fig. 1 for two extreme choices. The first option (labeled “Free+RSBL”) is to leave the normalization of reactor fluxes free and include the RSBL data. The second option (labeled “Huber”) is not to include short-baseline reactor data but assume reactor fluxes and uncertainties as predicted in [30].

From the results in the figure and table we conclude that:

1. if we define the 3σ relative precision of a parameter by $2(x^{\text{up}} - x^{\text{low}})/(x^{\text{up}} + x^{\text{low}})$, where x^{up} (x^{low}) is the upper (lower) bound on a parameter x at the 3σ level, from the numbers in the table we find 3σ relative precision of 14% (θ_{12}), 32% (θ_{23}), 15% (θ_{13}), 14% (Δm_{21}^2) and 11% ($|\Delta m_{3\ell}^2|$) for the various oscillation parameters;
2. for either choice of the reactor fluxes the global best fit corresponds to IO with $\sin^2 \theta_{23} > 0.5$, while the second local minima is for NO with $\sin^2 \theta_{23} < 0.5$;
3. the statistical significance of the preference for Inverted versus Normal ordering is quite small, $\Delta\chi^2 \lesssim 1$;
4. the present global analysis disfavors $\theta_{13} = 0$ with a $\Delta\chi^2 \approx 500$. Such impressive result is mostly driven by the reactor data from Daya Bay, with secondary contributions from RENO and Double Chooz;
5. the uncertainty on θ_{13} associated with the choice of reactor fluxes is at the level of 0.5σ in the global analysis. This is so because the most precise results from Daya Bay and RENO are independent of the reactor flux normalization;
6. a non-maximal value of the θ_{23} mixing is slightly favored, at the level of $\sim 1.4\sigma$ for Inverted Ordering at of $\sim 1.0\sigma$ for Normal Ordering;

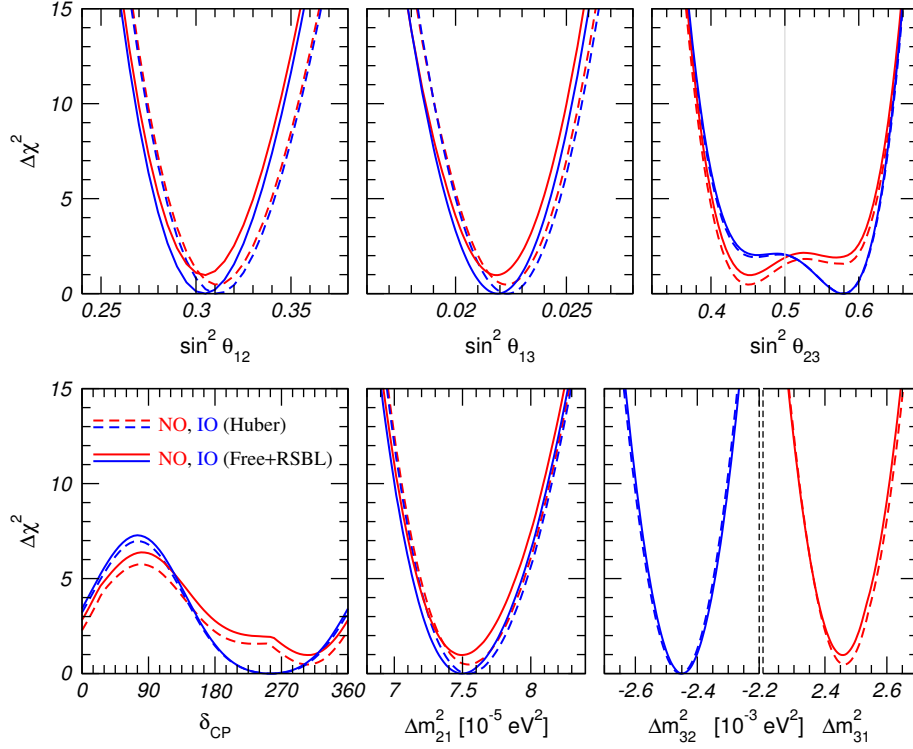


Fig. 1. Global 3ν oscillation analysis. The red (blue) curves are for Normal (Inverted) Ordering. For solid curves the normalization of reactor fluxes is left free and data from short-baseline (less than 100 m) reactor experiments are included. For dashed curves short-baseline data are not included but reactor fluxes as predicted in [30] are assumed. Note that as atmospheric mass-squared splitting we use Δm_{31}^2 for NO and Δm_{32}^2 for IO. Figure similar to Fig. 2 in Ref. [27].

7. the statistical significance of the preference of the fit for the second (first) octant of θ_{23} is $\leq 1.4\sigma$ ($\leq 1.0\sigma$) for IO (NO);
8. the best fit for δ_{CP} for all analyses and orderings occurs for $\delta_{\text{CP}} \approx 3\pi/2$, and values around $\pi/2$ are disfavored with $\Delta\chi^2 \simeq 6$. Assigning a confidence level to this $\Delta\chi^2$ is non-trivial, due to the non-Gaussian behavior of the involved χ^2 function, see Refs. [27, 40] for discussions and a Monte Carlo studies.

These results are robust with respect to changes in the statistical interpretation. The Bayesian analysis performed in [41] leads to quantitatively very similar results.

From this global analysis one can also derive the 3σ ranges on the magnitude of the elements of the leptonic mixing matrix to be:

$$|U| = \begin{pmatrix} 0.801 \rightarrow 0.845 & 0.514 \rightarrow 0.580 & 0.137 \rightarrow 0.158 \\ 0.225 \rightarrow 0.517 & 0.441 \rightarrow 0.699 & 0.614 \rightarrow 0.793 \\ 0.246 \rightarrow 0.529 & 0.464 \rightarrow 0.713 & 0.590 \rightarrow 0.776 \end{pmatrix}. \quad (7)$$

The present status of the determination of leptonic CP violation is further illustrated in Fig. 2. On the left panel we show the dependence of $\Delta\chi^2$ of the global analysis on the Jarlskog invariant which gives a convention-independent measure of CP violation [42], defined as:

$$\text{Im} [U_{\alpha i} U_{\alpha j}^* U_{\beta i}^* U_{\beta j}] \equiv \cos \theta_{12} \sin \theta_{12} \cos \theta_{23} \sin \theta_{23} \cos^2 \theta_{13} \sin \theta_{13} \sin \delta_{\text{CP}} \equiv J_{\text{CP}}^{\text{max}} \sin \delta_{\text{CP}} \quad (8)$$

where we have used the parametrization in Eq. (4). Thus the determination of the mixing angles yields at present a maximum allowed CP violation

$$J_{\text{CP}}^{\text{max}} = 0.0329 \pm 0.0009 (\pm 0.0027) \quad (9)$$

	Normal Ordering ($\Delta\chi^2 = 0.97$)		Inverted Ordering (best fit)		Any Ordering
	bfp $\pm 1\sigma$	3σ range	bfp $\pm 1\sigma$	3σ range	3σ range
$\sin^2 \theta_{12}$	$0.304^{+0.013}_{-0.012}$	0.270 \rightarrow 0.344	$0.304^{+0.013}_{-0.012}$	0.270 \rightarrow 0.344	0.270 \rightarrow 0.344
$\theta_{12}/^\circ$	$33.48^{+0.78}_{-0.75}$	31.29 \rightarrow 35.91	$33.48^{+0.78}_{-0.75}$	31.29 \rightarrow 35.91	31.29 \rightarrow 35.91
$\sin^2 \theta_{23}$	$0.452^{+0.052}_{-0.028}$	0.382 \rightarrow 0.643	$0.579^{+0.025}_{-0.037}$	0.389 \rightarrow 0.644	0.385 \rightarrow 0.644
$\theta_{23}/^\circ$	$42.3^{+3.0}_{-1.6}$	38.2 \rightarrow 53.3	$49.5^{+1.5}_{-2.2}$	38.6 \rightarrow 53.3	38.3 \rightarrow 53.3
$\sin^2 \theta_{13}$	$0.0218^{+0.0010}_{-0.0010}$	0.0186 \rightarrow 0.0250	$0.0219^{+0.0011}_{-0.0010}$	0.0188 \rightarrow 0.0251	0.0188 \rightarrow 0.0251
$\theta_{13}/^\circ$	$8.50^{+0.20}_{-0.21}$	7.85 \rightarrow 9.10	$8.51^{+0.20}_{-0.21}$	7.87 \rightarrow 9.11	7.87 \rightarrow 9.11
$\delta_{\text{CP}}/^\circ$	306^{+39}_{-70}	0 \rightarrow 360	254^{+63}_{-62}	0 \rightarrow 360	0 \rightarrow 360
$\frac{\Delta m_{21}^2}{10^{-5} \text{ eV}^2}$	$7.50^{+0.19}_{-0.17}$	7.02 \rightarrow 8.09	$7.50^{+0.19}_{-0.17}$	7.02 \rightarrow 8.09	7.02 \rightarrow 8.09
$\frac{\Delta m_{3\ell}^2}{10^{-3} \text{ eV}^2}$	$+2.457^{+0.047}_{-0.047}$	+2.317 \rightarrow +2.607	$-2.449^{+0.048}_{-0.047}$	-2.590 \rightarrow -2.307	$\left[\begin{array}{l} +2.325 \rightarrow +2.599 \\ -2.590 \rightarrow -2.307 \end{array} \right]$

Table 2. Three-flavor oscillation parameters from our fit to global data after the NOW 2014 conference [27]. The results are presented for the “Free Fluxes + RSBL” in which reactor fluxes have been left free in the fit and short baseline reactor data (RSBL) with $L \lesssim 100$ m are included. The numbers in the 1st (2nd) column are obtained assuming NO (IO), *i.e.*, relative to the respective local minimum, whereas in the 3rd column we minimize also with respect to the ordering. Note that $\Delta m_{3\ell}^2 \equiv \Delta m_{31}^2 > 0$ for NO and $\Delta m_{3\ell}^2 \equiv \Delta m_{32}^2 < 0$ for IO.

at 1σ (3σ) for both orderings. The preference of the present data for non-zero δ_{CP} implies a best fit $J_{\text{CP}}^{\text{best}} = -0.032$, which is favored over CP conservation at the $\sim 1.2\sigma$ level. These numbers can be compared with the size of the Jarlskog invariant in the quark sector, which is determined to be $J_{\text{CP}}^{\text{quarks}} = (3.06^{+0.21}_{-0.20}) \times 10^{-5}$ [24].

In the right panel of Fig. 2 we recast the allowed regions for the leptonic mixing matrix in terms of one leptonic unitarity triangle. Since in the analysis U is unitary by construction, any given pair of rows or columns can be used to define a triangle in the complex plane. In the figure we show the triangle corresponding to the unitarity conditions on the first and third columns which is the leptonic analogous to the one usually showed for the quark sector. In this figure the absence of CP violation implies a flat triangle, *i.e.*, $\text{Im}(z) = 0$. As can be seen, the horizontal axis marginally crosses the 1σ allowed region, which for 2 dof corresponds to $\Delta\chi^2 \simeq 2.3$. This is consistent with the present preference for CP violation, $\chi^2(J_{\text{CP}} = 0) - \chi^2(J_{\text{CP}} \text{ free}) = 1.5$. A detailed discussion of the status of the CP phase from present data can be found in Ref. [40].

3. Absolute neutrino mass measurements

Oscillation experiments provide information on the mass-squared splittings Δm_{ij}^2 and on the leptonic mixing angles U_{ij} , but they are insensitive to the absolute mass scale for the neutrinos. Of course, the results of an oscillation experiment do provide a lower bound on the heavier mass in Δm_{ij}^2 , $|m_i| \geq \sqrt{\Delta m_{ij}^2}$ for $\Delta m_{ij}^2 > 0$, but there is no upper bound on this mass. In particular, the corresponding neutrinos could be approximately degenerate at a mass scale that is much higher than $\sqrt{\Delta m_{ij}^2}$. Moreover, there is neither an upper nor a lower bound on the lighter mass m_j .

Information on the neutrino masses, rather than mass differences, can be extracted from kinematic studies of reactions in which a neutrino or an anti-neutrino is involved. In the presence of mixing the most relevant constraint comes from the study of the end point ($E \sim E_0$) of the electron spectrum in Tritium beta decay ${}^3\text{H} \rightarrow {}^3\text{He} + e^- + \bar{\nu}_e$. This spectrum can be effectively described by a single parameter, m_{ν_e} , if for all

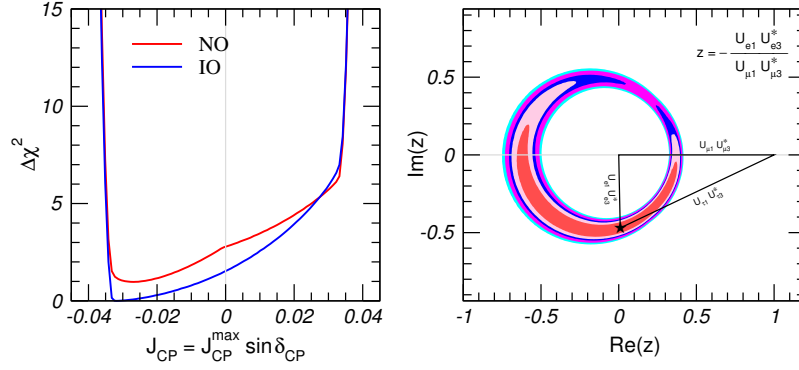


Fig. 2. Left: dependence of the global $\Delta\chi^2$ function on the Jarlskog invariant. The red (blue) curves are for NO (IO). Right: leptonic unitarity triangle. After scaling and rotating so that two of its vertices always coincide with $(0,0)$ and $(1,0)$ we plot the 1σ , 90% , 2σ , 99% , 3σ CL (2 dof) allowed regions of the third vertex.

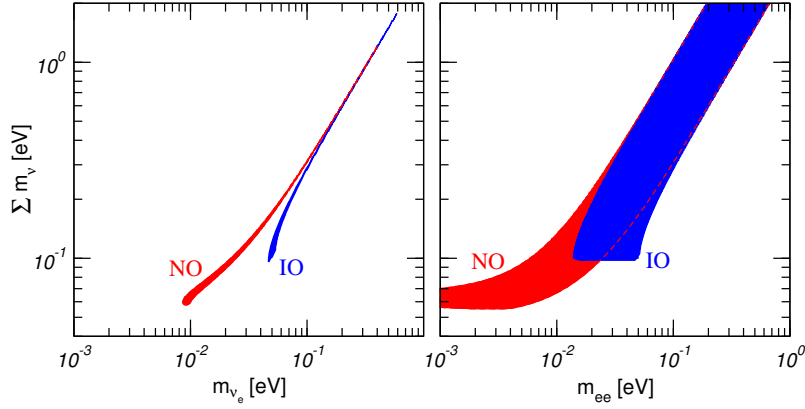


Fig. 3. 95% allowed regions (for 2 dof) in the planes $(m_{\nu_e}, \Sigma m_\nu)$ and $(m_{ee}, \Sigma m_\nu)$ obtain from projecting the results of the global analysis of oscillation data.

neutrino states $E_0 - E \gg m_i$. In this case:

$$\frac{dN}{dE} \simeq R(E) \sum_i |U_{ei}|^2 \sqrt{(E_0 - E)^2 - m_{\nu_e}^2}, \quad (10)$$

where $R(E)$ contains all the m_ν -independent factors, and

$$m_{\nu_e}^2 = \frac{\sum_i m_i^2 |U_{ei}|^2}{\sum_i |U_{ei}|^2} = \sum_i m_i^2 |U_{ei}|^2 = c_{13}^2 c_{12}^2 m_1^2 + c_{13}^2 s_{12}^2 m_2^2 + s_{13}^2 m_3^2, \quad (11)$$

where the second equality holds if unitarity is assumed. At present we only have an upper bound, $m_{\nu_e} \leq 2.2$ eV at 95% CL [43], which is expected to be superseded soon by KATRIN [44] with about one order of magnitude improvement in sensitivity.

Direct information on neutrino masses can also be obtained from neutrinoless double beta decay $(A, Z) \rightarrow (A, Z+2) + e^- + e^-$. This process violates lepton number by two units, hence in order to induce the $0\nu\beta\beta$ decay ν 's must Majorana particles. In particular, for the case in which the only effective lepton number violation at low energies is induced by the Majorana mass term for the neutrinos, the rate of $0\nu\beta\beta$ decay is proportional to the *effective Majorana mass* of ν_e :

$$m_{ee} = \left| \sum_i m_i U_{ei}^2 \right| = \left| m_1 c_{13}^2 c_{12}^2 e^{i2\alpha_1} + m_2 c_{13}^2 s_{12}^2 e^{i2\alpha_2} + m_3 s_{13}^2 e^{-i2\delta_{CP}} \right| \quad (12)$$

which, unlike Eq. (11), depends also on the three CP violating phases. Recent searches carried out with ^{76}Ge (GERDA experiment [45]) and ^{136}Xe (KamLAND-Zen [46] and EXO-200 [47] experiments) have established the lifetime of this decay to be longer than 10^{25} yr, corresponding to a limit on the neutrino mass of $m_{ee} \leq 0.2 - 0.4$ eV at 90% CL. A series of new experiments is planned with sensitivity of up to $m_{ee} \sim 0.01$ eV [48].

Neutrino masses have also interesting cosmological effects. In general, cosmological data mostly give information on the sum of the neutrino masses, $\sum_i m_i$, while they have very little to say on their mixing structure and on the ordering of the mass states.

Correlated information on these three probes of the neutrino mass scale can be obtained by mapping the results from the global analysis of oscillations presented previously. We show in Fig. 3 the present status of this exercise. The relatively large width of the regions in the right panel are due to the unknown Majorana phases. Thus from a positive determination of two of these probes information can be obtained on the value of the Majorana phases and/or the mass ordering.

4. Sterile neutrinos at the eV scale

Besides the huge success of three-flavour oscillations described in Sec. 2 there are some anomalies which cannot be explained within the 3ν framework and which might point towards the existence of additional neutrino flavors (so-called sterile neutrinos) with masses at the eV scale:

- the LSND experiment [49] reports evidence for $\bar{\nu}_\mu \rightarrow \bar{\nu}_e$ transitions with $E/L \sim 1$ eV², where E and L are the neutrino energy and the distance between source and detector, respectively;
- this effect is also searched for by the MiniBooNE experiment [50], which reports a yet unexplained event excess in the low-energy region of the electron neutrino and anti-neutrino event spectra. No significant excess is found at higher neutrino energies. Interpreting the data in terms of oscillations, parameter values consistent with the ones from LSND are obtained;
- radioactive source experiments at the Gallium solar neutrino experiments SAGE and GALLEX have obtained an event rate which is somewhat lower than expected. This effect can be explained by the hypothesis of ν_e disappearance due to oscillations with $\Delta m^2 \gtrsim 1$ eV² (“Gallium anomaly”) [51, 52];
- state-of-the-art calculations of the neutrino flux emitted by nuclear reactors [29, 30] predict a neutrino rate which is a few percent higher than observed in short-baseline ($L \lesssim 100$ m) reactor experiments. A decreased rate at those distances can be explained by assuming $\bar{\nu}_e$ disappearance due to oscillations with $\Delta m^2 \sim 1$ eV² (“reactor anomaly”) [53].

Here we report the results of a global analysis from Ref. [54] of those data under the hypothesis of additional neutrino species at the eV scale (see [55, 56] for similar analyses). We introduce a neutrino state, ν_4 , with a mass-squared difference Δm_{41}^2 much larger than $|\Delta m_{31}^2|$. This situation is called “3+1 mass scheme”. In this case the oscillation probabilities for experiments exploring the range $E/L \sim 1$ eV² are rather simple:

$$P_{\alpha\alpha} = 1 - \sin^2 2\theta_{\alpha\alpha} \sin^2 \Delta, \quad P_{\mu e} = \sin^2 2\theta_{\mu e} \sin^2 \Delta, \quad (13)$$

where $\Delta \equiv \Delta m_{41}^2 L/4E$ and the effective mixing angles are defined as

$$\sin^2 2\theta_{\alpha\alpha} \equiv 4|U_{\alpha 4}|^2(1 - |U_{\alpha 4}|^2), \quad \sin^2 2\theta_{\mu e} \equiv 4|U_{\mu 4}|^2|U_{e 4}|^2, \quad (14)$$

with $\alpha = e, \mu$ and $U_{\alpha 4}$ are the elements of the lepton mixing matrix describing the mixing of the 4th neutrino mass state with the electron and muon flavour. There is no CP violation in 3+1 SBL oscillations and those relations apply for neutrinos as well as antineutrinos. Neglecting quadratic terms in the mixing matrix elements one has the following relation between the effective amplitudes relevant for appearance and disappearance probabilities:

$$4 \sin^2 2\theta_{\mu e} \approx \sin^2 2\theta_{ee} \sin^2 2\theta_{\mu\mu}. \quad (15)$$

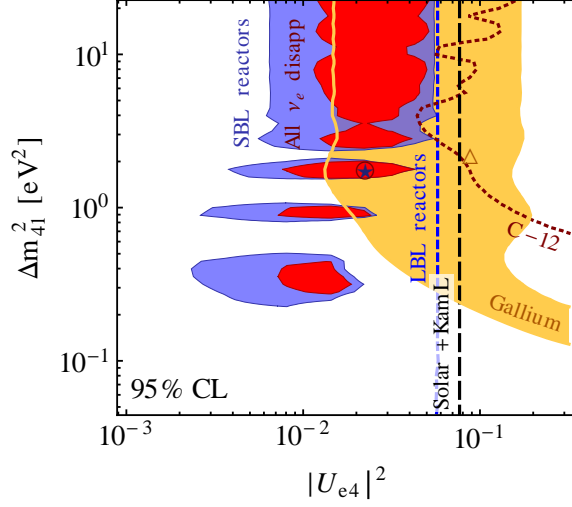


Fig. 4. Allowed regions at 95% CL (2 dof) for 3+1 oscillations. We show SBL reactor data [31–39] (blue shaded), Gallium radioactive source data [6, 57–59] (orange shaded), ν_e disappearance constraints from ν_e - ^{12}C scattering data from LSND and KARMEN [60, 61] (dark red dotted), long-baseline reactor data from CHOOZ, Palo Verde, DoubleChooz, Daya Bay and RENO (blue short-dashed) and solar+KamLAND data (black long-dashed). The red shaded region is the combined region from all these ν_e and $\bar{\nu}_e$ disappearance data sets. See Ref. [54] for details.

Dividing the relevant data into ν_e disappearance, ν_μ disappearance, and $\nu_\mu \rightarrow \nu_e$ appearance searches, this relation implies that the system is over-constrained. Indeed, as will be discussed below, there is significant tension in the global data and Eq. (15) makes it difficult to obtain a good fit to all available data.

We consider first the global data including SBL anomalies related to $\bar{\nu}_e$ and ν_e disappearance (reactor and Gallium anomalies) but ignoring for the time being the $\nu_\mu \rightarrow \nu_e$ and $\bar{\nu}_\mu \rightarrow \bar{\nu}_e$ appearance anomalies (LSND and MiniBooNE). In this case the relevant SBL phenomenology is determined by the two parameters Δm_{41}^2 and $|U_{e4}|$. The allowed regions for them is shown in Fig. 4. We find that a consistent region emerges (shown in red), not in conflict with any other data. The best fit point occurs at $\sin^2 2\theta_{ee} = 0.09$ and $\Delta m_{41}^2 = 1.78 \text{ eV}^2$, and the no-oscillation hypothesis for the eV-scale is excluded at 3.1σ ($\Delta\chi^2 = 12.9/2$ dof), driven by the reactor and Gallium anomalies. The θ_{13} determination is rather stable with respect to the presence of sterile neutrinos, up to an ambiguity at the level of less than 1σ (see also discussion in section 2). We note, however, that its interpretation becomes slightly more complicated. For instance, using a particular parametrization [54] for the 3+1 scheme, the relation between mixing matrix elements and mixing angles is $|U_{e3}| = \cos \theta_{14} \sin \theta_{13}$ and $|U_{e4}| = \sin \theta_{14}$. Hence, the one-to-one correspondence between $|U_{e3}|$ and θ_{13} as in the three-flavor case is spoiled.

We now address the question whether the hints for ν_e disappearance can be reconciled with the appearance hints from LSND and MiniBooNE. As mentioned above, Eq. (15) links those appearance signals to disappearance in the ν_e as well as ν_μ channels. Despite the possible signal in ν_e disappearance, so-far no positive signal has been observed in ν_μ disappearance and several experiments set bounds on the relevant mixing parameter $|U_{\mu 4}|$, see Fig. 5 (left). Hence, the combined limits on ν_μ and ν_e mixing with the eV-scale mass state lead to a tension between appearance signals and disappearance data in the 3+1 scheme. Such tension is illustrated for global data in the right panel of Fig. 5, where we show the allowed region for all appearance experiments, compared to the limit from disappearance experiments in the plane of $\sin^2 2\theta_{\mu e}$ and Δm_{41}^2 . The preferred values of Δm_{41}^2 for disappearance data come from the reactor and Gallium anomalies. The regions for disappearance data, however, are not closed in this projection in the parameter space and include $\sin^2 2\theta_{\mu e} = 4|U_{e4}U_{\mu 4}|^2 = 0$, which can always be achieved by letting $U_{\mu 4} \rightarrow 0$ due to the non-observation of any positive signal in SBL ν_μ disappearance. The upper bound on $\sin^2 2\theta_{\mu e}$ from disappearance emerges essentially as the product of the upper bounds on $|U_{e4}|$ and $|U_{\mu 4}|$ from ν_e and ν_μ disappearance according to Eq. (15). We observe from the plot the clear tension between those data sets, with only marginal overlap

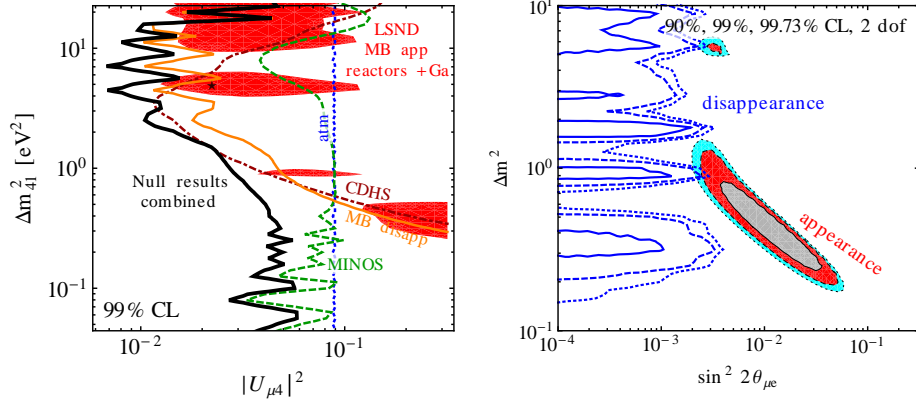


Fig. 5. Left: Constraints in the plane of $|U_{\mu 4}|^2$ and Δm_{41}^2 at 99% CL (2 dof) from CDHS [62], atmospheric neutrinos [63], MiniBooNE disappearance [64], MINOS CC and NC data [65, 66], and the combination of them. In red we show the region preferred by LSND and MiniBooNE appearance data combined with reactor and Gallium data, where for fixed $|U_{\mu 4}|^2$ we minimize with respect to $|U_{e 4}|^2$. Right: Comparison of the parameter region preferred by appearance data (LSND [49], MiniBooNE appearance analysis [50], NOMAD [67], KARMEN [68], ICARUS [69], E776 [70]) to the exclusion limit from disappearance data (atmospheric, solar, reactors, Gallium, CDHS, MINOS, MiniBooNE disappearance, KARMEN and LSND $\nu_e - ^{12}\text{C}$ scattering). See Ref. [54] for details.

regions at above 99% CL around $\Delta m_{41}^2 \approx 0.9 \text{ eV}^2$ and at 3σ around $\Delta m_{41}^2 \approx 6 \text{ eV}^2$. We find that the global 3+1 fit leads to $\chi_{\text{min}}^2/\text{dof} = 712/680$ with a p-value 19%, whereas the so-called parameter goodness of fit (PG) test [71] indicates that appearance and disappearance data are consistent with each other only with a p-value of about 10^{-4} .

A valid question to ask is whether the situation improves if more neutrino states at the eV scale are introduced. Consider the hypothesis of 2 states with eV scale mass splittings, ν_4 and ν_5 , which can be arranged either such that Δm_{41}^2 and Δm_{51}^2 are both positive (“3+2”) and where one of them is negative (“1+3+1”). The new qualitative feature in those 5-neutrino schemes is CP violation at the $E/L \sim \text{eV}^2$ scale [72, 73], which introduces some freedom in fitting neutrino versus anti-neutrino data from LSND and MiniBooNE together. However, the main prediction from the 4-neutrino case remains valid also for 5-neutrinos: a non-zero $\nu_\mu \rightarrow \nu_e$ appearance at SBL necessarily predicts SBL disappearance for ν_e as well as ν_μ . Indeed, the tension between appearance and disappearance data remains severe, and a PG analysis gives a consistency below 10^{-4} for 3+2, whereas for 1+3+1 consistency at the 2 permil level can be achieved [54].

In summary, several anomalies at the level of 3σ do not fit into the three-flavour picture and might indicate additional neutrino states at the eV scale. While a consistent fit can be obtained for data on ν_e disappearance (reactor and Gallium anomalies) the global data suffers from severe tension between appearance and disappearance data, mostly due to the non-observation of ν_μ disappearance at the eV^2 scale. Finally we mention that additional neutrino states with eV-like masses and sizeable mixings (as necessary to explain the oscillation anomalies) have severe implications for cosmology [74, 75] and may lead to observable effects in IceCube [76–78].

5. Matter potential: non-standard interactions

Neutrino oscillation experiments can also provide important information on other neutrino properties beyond the SM. As an example we briefly summarize here the results of the most up-to-date determination of new physics in the matter effects in neutrino propagation from the global analysis of neutrino oscillation experiments from Ref. [79], to which we refer the reader for details and related references.

In the three-flavor oscillation picture described above the neutrino evolution equation along trajectory parametrized by coordinate x reads ($\vec{\nu} = (\nu_e, \nu_\mu, \nu_\tau)^T$):

$$i \frac{d}{dx} \vec{\nu} = (H_{\text{vac}} + H_{\text{mat}}) \vec{\nu} \quad \text{with} \quad H_{\text{vac}} = U D_{\text{vac}} U^\dagger, \quad D_{\text{vac}} = \frac{1}{2E_\nu} \text{diag}(0, \Delta m_{21}^2, \Delta m_{31}^2) \quad (16)$$

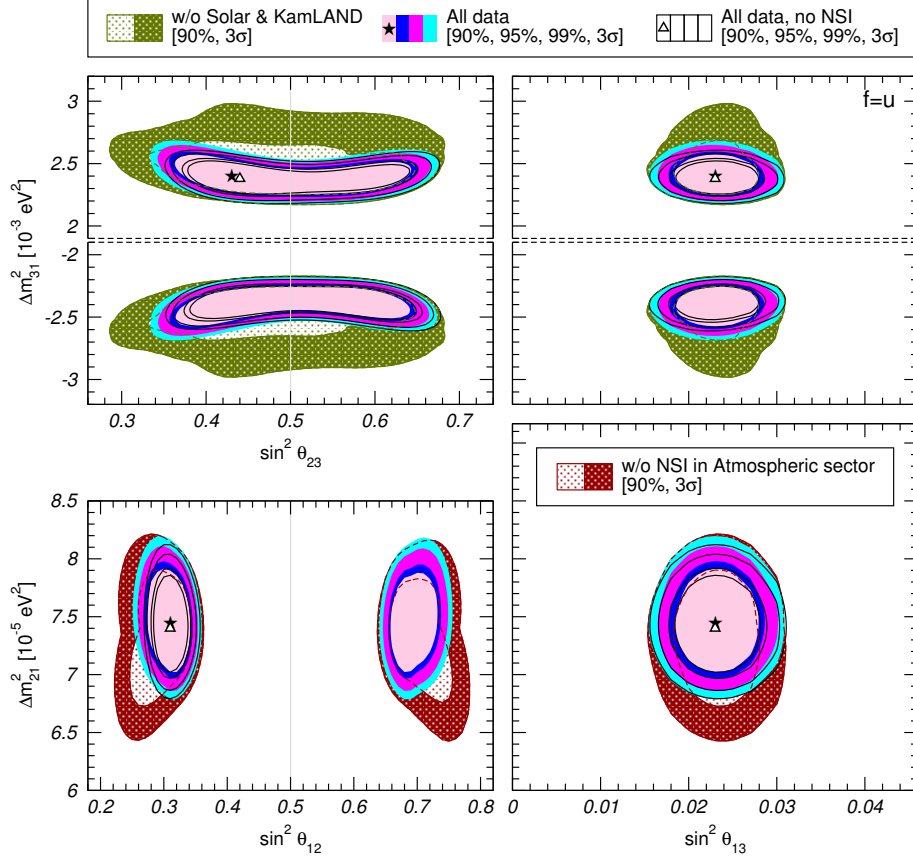


Fig. 6. Two-dimensional projections of the 90%, 95%, 99% and 3σ CL (2 dof) allowed regions of the oscillation parameters for $f = u$ after marginalizing over the matter potential parameters and the undisplayed oscillation parameters. The full regions and the star correspond to the global analysis including NSI, while the black-contour void regions and the triangle correspond to the analysis with the usual SM potential. The green and red dotted areas show the 90% and 3σ CL allowed regions from partial analyses where the effects of the non-standard matter potential have been neglected either in the solar+KamLAND (green) or in the atmospheric+LBL (red) sectors.

while for antineutrinos the hamiltonian is $H^{\bar{\nu}} = (H_{\text{vac}} - H_{\text{mat}})^*$. In the Standard Model H_{mat} is fully determined both in its strength and flavor structure to be $H_{\text{mat}}^{\text{SM}} = \sqrt{2}G_F N_e(r) \text{diag}(1, 0, 0)$ for ordinary matter [80, 81]. Generically ordinary matter is composed by electrons (e), up-quarks (u) and down-quark (d), thus in the most general case a non-standard matter potential can be parametrized as:

$$H_{\text{mat}} = \sqrt{2}G_F N_e(r) \begin{pmatrix} 1 & 0 & 0 \\ 0 & 0 & 0 \\ 0 & 0 & 0 \end{pmatrix} + \sqrt{2}G_F \sum_{f=e,u,d} N_f(r) \begin{pmatrix} \mathcal{E}_{ee}^f & \mathcal{E}_{e\mu}^f & \mathcal{E}_{e\tau}^f \\ \mathcal{E}_{e\mu}^{f*} & \mathcal{E}_{\mu\mu}^f & \mathcal{E}_{\mu\tau}^f \\ \mathcal{E}_{e\tau}^{f*} & \mathcal{E}_{\mu\tau}^{f*} & \mathcal{E}_{\tau\tau}^f \end{pmatrix}. \quad (17)$$

Since this matter term can be determined by oscillation experiments only up to an overall multiple of the identity, without loss of generality one can assume $\mathcal{E}_{\mu\mu}^f = 0$. With this, we have 8 additional parameters (for each f) since \mathcal{E}_{ee}^f and $\mathcal{E}_{\tau\tau}^f$ must be real whereas $\mathcal{E}_{e\mu}^f$, $\mathcal{E}_{e\tau}^f$ and $\mathcal{E}_{\mu\tau}^f$ can be complex.

The theoretical framework for this parametrization of the matter potential is provided by non-standard interactions (NSI) of neutrinos with the matter particles. They can be described by effective four-fermion operators of the form

$$\mathcal{L}_{\text{NSI}} = -2 \sqrt{2}G_F \varepsilon_{\alpha\beta}^{fP} (\bar{\nu}_\alpha \gamma^\mu \nu_\beta) (\bar{f} \gamma_\mu P f), \quad (18)$$

where f is a charged fermion, $P = (L, R)$ and $\varepsilon_{\alpha\beta}^{fP}$ are dimensionless parameters encoding the deviation from

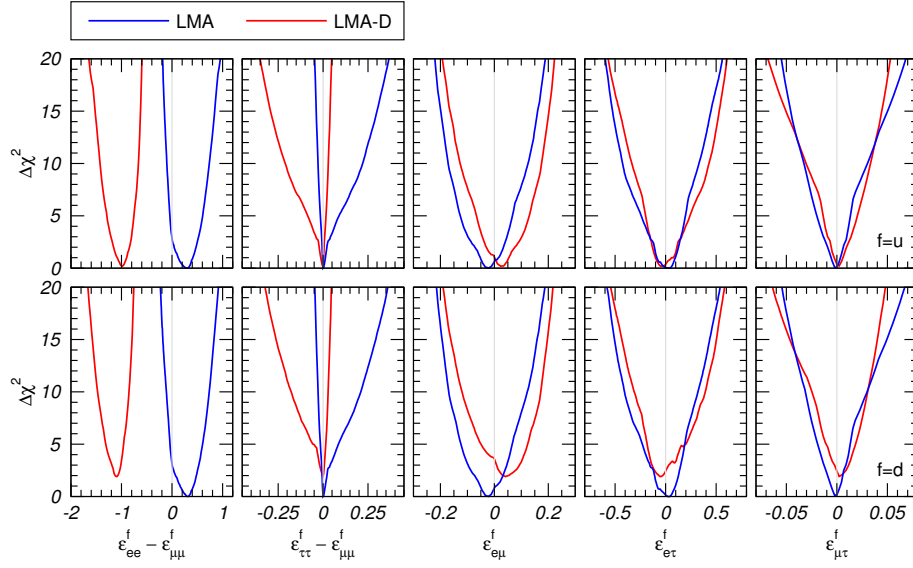


Fig. 7. Dependence of the $\Delta\chi^2$ function for the global analysis of solar, atmospheric, reactor and LBL data on the NSI parameters $\varepsilon_{\alpha\beta}^f$ for $f = u$ (upper panels) and $f = d$ (lower panels), for both LMA and LMA-D regions and the two variants of the SNO analysis, as labeled in the figure.

standard interactions. NSI enter in neutrino propagation only through the vector couplings so the induced matter Hamiltonian takes the form Eq. (17) with $\varepsilon_{\alpha\beta}^f = \varepsilon_{\alpha\beta}^{fL} + \varepsilon_{\alpha\beta}^{fR}$.

We show in Figs. 6 and 7 some projections of the large parameter space in oscillation parameters and on the NSI parameters (after marginalizing over all oscillation and NSI undisplayed parameters) from a global analysis of oscillation data in terms of 3ν oscillations with general real matter potential (with Δm_{21}^2 effects neglected in the analysis of ATM and LBL experiments). From the figures we read the following:

- the determination of most the oscillation parameters discussed in the previous section is robust under the presence of NSI as large as allowed by the oscillation data itself with the exception of the octant of θ_{12} ;
- a solution with $\theta_{12} > 45^\circ$ (the “so-called” LMA-D solution [82]) still provides a good fit to the data, as can be seen in the lower-left panel in Fig. 6. Such solution requires large NSI, which nevertheless are fully compatible with the bounds from atmospheric and LBL oscillation data;
- the analysis of solar and KamLAND data favours non-vanishing NSI to better fit the fact that neither the SNO nor SK4 low energy threshold analysis nor the ^8B measurement in Borexino seem to show evidence of the low energy turn-up of the spectrum predicted in the standard LMA MSW;
- comparing the results in Fig. 7 with the bounds on NSI derived in Refs. [83, 84] from non-oscillation data we find that, with the possible exception of $\varepsilon_{e\mu}^{u,d}$, the global oscillation analysis presented here yields the most restrictive bounds on the *vector* NSI parameters, in particular those involving τ flavour.

It is important to notice that in writing the phenomenological Lagrangian in Eq. (18) one assumes that the new physics which induces the NSI operators does not introduce new charge lepton physics at tree level or that charge lepton effects are very suppressed compared to those of neutrinos. This constraints the new physics realizations of this scenario [85] and, generically, the size of the NSI couplings which can be generated.

6. Conclusions and outlook

Thanks to the remarkable discoveries by neutrino oscillation experiments, such as those awarded by 2015 Nobel prize, it is now an established fact that neutrinos have mass and leptonic flavors are not symmetries of Nature. These results represent, to this date, the only laboratory evidence of physics beyond the Standard Model.

In this contribution we have summarized some results on the present characterization of the low energy parametrization of the neutrino properties as obtained from direct comparison with the data. The relevance of the work lies on the fact that the determination of the flavour structure of the leptons at low energies, is, at this point, our only source of information to understand the underlying new dynamics and it is fundamental to ultimately establish the *New Standard Model*.

Acknowledgments

This work is supported by Spanish MINECO grants FPA2012-31880, FPA2012-34694 and FPA2013-46570, by the Severo Ochoa program SEV-2012-0249 of IFT, by the Maria de Maeztu program MDM-2014-0369 of ICCUB, and consolidator-ingenio 2010 grant CSD-2008-0037, by CUR Generalitat de Catalunya grant 2014-SGR-104, by USA-NSF grant PHY-13-16617, and by EU grant FP7 ITN INVISIBLES (Marie Curie Actions PITN-GA-2011-289442).

References

- [1] B. Pontecorvo, Neutrino Experiments and the Problem of Conservation of Leptonic Charge, *Sov. Phys. JETP* 26 (1968) 984–988, [*Zh. Eksp. Teor. Fiz.* 53, 1717 (1967)].
- [2] V. N. Gribov, B. Pontecorvo, Neutrino astronomy and lepton charge, *Phys. Lett. B* 28 (1969) 493. doi:10.1016/0370-2693(69)90525-5.
- [3] M. C. Gonzalez-Garcia, M. Maltoni, Phenomenology with Massive Neutrinos, *Phys. Rept.* 460 (2008) 1–129. arXiv:0704.1800, doi:10.1016/j.physrep.2007.12.004.
- [4] R. Wendell, Atmospheric Results from Super-Kamiokande, talk given at the *XXVI International Conference on Neutrino Physics and Astrophysics*, Boston, USA, June 2–7, 2014.
- [5] B. T. Cleveland, T. Daily, R. Davis, Jr., J. R. Distel, K. Lande, C. K. Lee, P. S. Wildenhain, J. Ullman, Measurement of the solar electron neutrino flux with the Homestake chlorine detector, *Astrophys. J.* 496 (1998) 505–526. doi:10.1086/305343.
- [6] F. Kaether, W. Hampel, G. Heusser, J. Kiko, T. Kirsten, Reanalysis of the GALLEX solar neutrino flux and source experiments, *Phys. Lett. B* 685 (2010) 47–54. arXiv:1001.2731, doi:10.1016/j.physletb.2010.01.030.
- [7] J. N. Abdurashitov, et al., Measurement of the solar neutrino capture rate with gallium metal. III: Results for the 2002–2007 data-taking period, *Phys. Rev. C* 80 (2009) 015807. arXiv:0901.2200, doi:10.1103/PhysRevC.80.015807.
- [8] J. Hosaka, et al., Solar neutrino measurements in super-Kamiokande-I, *Phys. Rev. D* 73 (2006) 112001. arXiv:hep-ex/0508053, doi:10.1103/PhysRevD.73.112001.
- [9] J. P. Cravens, et al., Solar neutrino measurements in Super-Kamiokande-II, *Phys. Rev. D* 78 (2008) 032002. arXiv:0803.4312, doi:10.1103/PhysRevD.78.032002.
- [10] K. Abe, et al., Solar neutrino results in Super-Kamiokande-III, *Phys. Rev. D* 83 (2011) 052010. arXiv:1010.0118, doi:10.1103/PhysRevD.83.052010.
- [11] Y. Koshio, Solar Results from Super-Kamiokande, talk given at the *XXVI International Conference on Neutrino Physics and Astrophysics*, Boston, USA, June 2–7, 2014.
- [12] B. Aharmim, et al., Combined Analysis of all Three Phases of Solar Neutrino Data from the Sudbury Neutrino Observatory, *Phys. Rev. C* 88 (2013) 025501. arXiv:1109.0763, doi:10.1103/PhysRevC.88.025501.
- [13] G. Bellini, et al., Precision measurement of the 7Be solar neutrino interaction rate in Borexino, *Phys. Rev. Lett.* 107 (2011) 141302. arXiv:1104.1816, doi:10.1103/PhysRevLett.107.141302.
- [14] G. Bellini, et al., Measurement of the solar 8B neutrino rate with a liquid scintillator target and 3 MeV energy threshold in the Borexino detector, *Phys. Rev. D* 82 (2010) 033006. arXiv:0808.2868, doi:10.1103/PhysRevD.82.033006.
- [15] P. Adamson, et al., Measurement of Neutrino and Antineutrino Oscillations Using Beam and Atmospheric Data in MINOS, *Phys. Rev. Lett.* 110 (25) (2013) 251801. arXiv:1304.6335, doi:10.1103/PhysRevLett.110.251801.
- [16] K. Abe, et al., Precise Measurement of the Neutrino Mixing Parameter θ_{23} from Muon Neutrino Disappearance in an Off-Axis Beam, *Phys. Rev. Lett.* 112 (18) (2014) 181801. arXiv:1403.1532, doi:10.1103/PhysRevLett.112.181801.
- [17] M. Sanchez, Results and prospects from the NOvA experiment, talk given at the *XVII International Workshop on Neutrino Factories and Future Neutrino Facilities*, Rio de Janeiro, Brazil, August 10–15, 2015.
- [18] P. Adamson, et al., Electron neutrino and antineutrino appearance in the full MINOS data sample, *Phys. Rev. Lett.* 110 (17) (2013) 171801. arXiv:1301.4581, doi:10.1103/PhysRevLett.110.171801.
- [19] K. Abe, et al., Observation of Electron Neutrino Appearance in a Muon Neutrino Beam, *Phys. Rev. Lett.* 112 (2014) 061802. arXiv:1311.4750, doi:10.1103/PhysRevLett.112.061802.

- [20] Y. Abe, et al., Reactor electron antineutrino disappearance in the Double Chooz experiment, Phys. Rev. D86 (2012) 052008. [arXiv:1207.6632](#), [doi:10.1103/PhysRevD.86.052008](#).
- [21] C. Zhang, Recent Results From Daya Bay, talk given at the *XXVI International Conference on Neutrino Physics and Astrophysics*, Boston, USA, June 2–7, 2014.
- [22] J. H. Choi, et al., Observation of Energy and Baseline Dependent Reactor Antineutrino Disappearance in the RENO Experiment [arXiv:1511.05849](#).
- [23] A. Gando, et al., Constraints on θ_{13} from A Three-Flavor Oscillation Analysis of Reactor Antineutrinos at KamLAND, Phys. Rev. D83 (2011) 052002. [arXiv:1009.4771](#), [doi:10.1103/PhysRevD.83.052002](#).
- [24] K. A. Olive, et al., Review of Particle Physics, Chin. Phys. C38 (2014) 090001. [doi:10.1088/1674-1137/38/9/090001](#).
- [25] F. Capozzi, G. L. Fogli, E. Lisi, A. Marrone, D. Montanino, A. Palazzo, Status of three-neutrino oscillation parameters, circa 2013, Phys. Rev. D89 (2014) 093018. [arXiv:1312.2878](#), [doi:10.1103/PhysRevD.89.093018](#).
- [26] D. V. Forero, M. Tortola, J. W. F. Valle, Neutrino oscillations refitted, Phys. Rev. D90 (9) (2014) 093006. [arXiv:1405.7540](#), [doi:10.1103/PhysRevD.90.093006](#).
- [27] M. C. Gonzalez-Garcia, M. Maltoni, T. Schwetz, Updated fit to three neutrino mixing: status of leptonic CP violation, JHEP 11 (2014) 052. [arXiv:1409.5439](#), [doi:10.1007/JHEP11\(2014\)052](#).
- [28] M. Gonzalez-Garcia, M. Maltoni, T. Schwetz, NuFIT 2.0 (2014), <http://www.nu-fit.org>.
- [29] T. A. Mueller, et al., Improved Predictions of Reactor Antineutrino Spectra, Phys. Rev. C83 (2011) 054615. [arXiv:1101.2663](#), [doi:10.1103/PhysRevC.83.054615](#).
- [30] P. Huber, On the determination of anti-neutrino spectra from nuclear reactors, Phys. Rev. C84 (2011) 024617, [Erratum: Phys. Rev. C85,029901(2012)]. [arXiv:1106.0687](#), [doi:10.1103/PhysRevC.85.029901](#), [doi:10.1103/PhysRevC.84.024617](#).
- [31] Y. Declais, et al., Study of reactor anti-neutrino interaction with proton at Bugey nuclear power plant, Phys. Lett. B338 (1994) 383–389. [doi:10.1016/0370-2693\(94\)91394-3](#).
- [32] A. A. Kuvshinnikov, L. A. Mikaelyan, S. V. Nikolaev, M. D. Skorokhvatov, A. V. Etenko, Measuring the anti-electron-neutrino $+p \rightarrow n + e^+$ cross-section and beta decay axial constant in a new experiment at Rovno NPP reactor. (In Russian), JETP Lett. 54 (1991) 253–257, [Sov. J. Nucl. Phys.52,300(1990)].
- [33] Y. Declais, et al., Search for neutrino oscillations at 15-meters, 40-meters, and 95-meters from a nuclear power reactor at Bugey, Nucl. Phys. B434 (1995) 503–534. [doi:10.1016/0550-3213\(94\)00513-E](#).
- [34] G. S. Vidyakin, V. N. Vyrodov, I. I. Gurevich, Yu. V. Kozlov, V. P. Martemyanov, S. V. Sukhotin, V. G. Tarasenkov, S. K. Khakimov, Detection of Anti-neutrinos in the Flux From Two Reactors, Sov. Phys. JETP 66 (1987) 243–247, [Zh. Eksp. Teor. Fiz.93,424(1987)].
- [35] G. S. Vidyakin, et al., Limitations on the characteristics of neutrino oscillations, JETP Lett. 59 (1994) 390–393, [Pisma Zh. Eksp. Teor. Fiz.59,364(1994)].
- [36] H. Kwon, F. Boehm, A. A. Hahn, H. E. Henrikson, J. L. Vuilleumier, J. F. Cavaignac, D. H. Koang, B. Vignon, F. Von Feilitzsch, R. L. Mossbauer, Search for Neutrino Oscillations at a Fission Reactor, Phys. Rev. D24 (1981) 1097–1111. [doi:10.1103/PhysRevD.24.1097](#).
- [37] G. Zacek, et al., Neutrino Oscillation Experiments at the Gosgen Nuclear Power Reactor, Phys. Rev. D34 (1986) 2621–2636. [doi:10.1103/PhysRevD.34.2621](#).
- [38] Z. D. Greenwood, et al., Results of a two position reactor neutrino oscillation experiment, Phys. Rev. D53 (1996) 6054–6064. [doi:10.1103/PhysRevD.53.6054](#).
- [39] A. I. Afonin, S. N. Ketov, V. I. Kopeikin, L. A. Mikaelyan, M. D. Skorokhvatov, S. V. Tolokonnikov, A Study of the Reaction $\bar{\nu}_e + P \rightarrow e^+ + N$ on a Nuclear Reactor, Sov. Phys. JETP 67 (1988) 213–221, [Zh. Eksp. Teor. Fiz.94N2,1(1988)].
- [40] J. Elefant, T. Schwetz, On the determination of the leptonic CP phase, JHEP 09 (2015) 016. [arXiv:1506.07685](#), [doi:10.1007/JHEP09\(2015\)016](#).
- [41] J. Bergstrom, M. C. Gonzalez-Garcia, M. Maltoni, T. Schwetz, Bayesian global analysis of neutrino oscillation data, JHEP 09 (2015) 200. [arXiv:1507.04366](#), [doi:10.1007/JHEP09\(2015\)200](#).
- [42] C. Jarlskog, Commutator of the Quark Mass Matrices in the Standard Electroweak Model and a Measure of Maximal CP Violation, Phys. Rev. Lett. 55 (1985) 1039. [doi:10.1103/PhysRevLett.55.1039](#).
- [43] J. Bonn, et al., The Mainz neutrino mass experiment, Nucl. Phys. Proc. Suppl. 91 (2001) 273–279, [PoSHeP2001,192(2001)]. [doi:10.1016/S0920-5632\(00\)00951-8](#).
- [44] A. Osipowicz, et al., KATRIN: A Next generation tritium beta decay experiment with sub-eV sensitivity for the electron neutrino mass. Letter of intent [arXiv:hep-ex/0109033](#).
- [45] M. Agostini, et al., Results on Neutrinoless Double- β Decay of ^{76}Ge from Phase I of the GERDA Experiment, Phys. Rev. Lett. 111 (12) (2013) 122503. [arXiv:1307.4720](#), [doi:10.1103/PhysRevLett.111.122503](#).
- [46] A. Gando, et al., Limit on Neutrinoless $\beta\beta$ Decay of ^{136}Xe from the First Phase of KamLAND-Zen and Comparison with the Positive Claim in ^{76}Ge , Phys. Rev. Lett. 110 (6) (2013) 062502. [arXiv:1211.3863](#), [doi:10.1103/PhysRevLett.110.062502](#).
- [47] J. B. Albert, et al., Search for Majorana neutrinos with the first two years of EXO-200 data, Nature 510 (2014) 229–234. [arXiv:1402.6956](#), [doi:10.1038/nature13432](#).
- [48] J. J. Gomez-Cadenas, J. Martin-Albo, M. Mezzetto, F. Monrabal, M. Sorel, The Search for neutrinoless double beta decay, Riv. Nuovo Cim. 35 (2012) 29–98. [arXiv:1109.5515](#), [doi:10.1393/ncr/i2012-10074-9](#).
- [49] A. Aguilar-Arevalo, et al., Evidence for neutrino oscillations from the observation of anti-neutrino(electron) appearance in a anti-neutrino(muon) beam, Phys. Rev. D64 (2001) 112007. [arXiv:hep-ex/0104049](#), [doi:10.1103/PhysRevD.64.112007](#).
- [50] A. Aguilar-Arevalo, et al., A Combined $\nu_\mu \rightarrow \nu_e$ and $\bar{\nu}_\mu \rightarrow \bar{\nu}_e$ Oscillation Analysis of the MiniBooNE Excesses [arXiv:1207.4809](#).
- [51] M. A. Acero, C. Giunti, M. Laveder, Limits on $\nu(e)$ and anti- $\nu(e)$ disappearance from Gallium and reactor experiments, Phys.

- Rev. D78 (2008) 073009. arXiv:0711.4222, doi:10.1103/PhysRevD.78.073009.
- [52] C. Giunti, M. Laveder, Statistical Significance of the Gallium Anomaly, Phys. Rev. C83 (2011) 065504. arXiv:1006.3244, doi:10.1103/PhysRevC.83.065504.
- [53] G. Mention, M. Fechner, T. Lasserre, T. A. Mueller, D. Lhuillier, M. Cribier, A. Letourneau, The Reactor Antineutrino Anomaly, Phys. Rev. D83 (2011) 073006. arXiv:1101.2755, doi:10.1103/PhysRevD.83.073006.
- [54] J. Kopp, P. A. N. Machado, M. Maltoni, T. Schwetz, Sterile Neutrino Oscillations: The Global Picture, JHEP 05 (2013) 050. arXiv:1303.3011, doi:10.1007/JHEP05(2013)050.
- [55] J. M. Conrad, C. M. Ignarra, G. Karagiorgi, M. H. Shaevitz, J. Spitz, Sterile Neutrino Fits to Short Baseline Neutrino Oscillation Measurements, Adv. High Energy Phys. 2013 (2013) 163897. arXiv:1207.4765, doi:10.1155/2013/163897.
- [56] C. Giunti, M. Laveder, Y. F. Li, H. W. Long, Pragmatic View of Short-Baseline Neutrino Oscillations, Phys. Rev. D88 (2013) 073008. arXiv:1308.5288, doi:10.1103/PhysRevD.88.073008.
- [57] W. Hampel, et al., Final results of the Cr-51 neutrino source experiments in GALLEX, Phys. Lett. B420 (1998) 114–126. doi:10.1016/S0370-2693(97)01562-1.
- [58] J. N. Abdurashitov, et al., Measurement of the response of the Russian-American gallium experiment to neutrinos from a Cr-51 source, Phys. Rev. C59 (1999) 2246–2263. arXiv:hep-ph/9803418, doi:10.1103/PhysRevC.59.2246.
- [59] J. N. Abdurashitov, et al., Measurement of the response of a Ga solar neutrino experiment to neutrinos from an Ar-37 source, Phys. Rev. C73 (2006) 045805. arXiv:nuc1-ex/0512041, doi:10.1103/PhysRevC.73.045805.
- [60] L. B. Auerbach, et al., Measurements of charged current reactions of nu(e) on 12-C, Phys. Rev. C64 (2001) 065501. arXiv:hep-ex/0105068, doi:10.1103/PhysRevC.64.065501.
- [61] B. Armbruster, et al., KARMEN limits on electron-neutrino \rightarrow tau-neutrino oscillations in two neutrino and three neutrino mixing schemes, Phys. Rev. C57 (1998) 3414–3424. arXiv:hep-ex/9801007, doi:10.1103/PhysRevC.57.3414.
- [62] F. Dydak, et al., A Search for Muon-neutrino Oscillations in the Δm^2 Range 0.3 eV² to 90 eV², Phys. Lett. B134 (1984) 281. doi:10.1016/0370-2693(84)90688-9.
- [63] R. Wendell, et al., Atmospheric neutrino oscillation analysis with sub-leading effects in Super-Kamiokande I, II, and III, Phys. Rev. D81 (2010) 092004. arXiv:1002.3471, doi:10.1103/PhysRevD.81.092004.
- [64] G. Cheng, et al., Dual baseline search for muon antineutrino disappearance at $0.1\text{eV}^2 < \Delta m^2 < 100\text{eV}^2$, Phys. Rev. D86 (2012) 052009. arXiv:1208.0322, doi:10.1103/PhysRevD.86.052009.
- [65] P. Adamson, et al., Search for sterile neutrino mixing in the MINOS long baseline experiment, Phys. Rev. D81 (2010) 052004. arXiv:1001.0336, doi:10.1103/PhysRevD.81.052004.
- [66] P. Adamson, et al., Active to sterile neutrino mixing limits from neutral-current interactions in MINOS, Phys. Rev. Lett. 107 (2011) 011802. arXiv:1104.3922, doi:10.1103/PhysRevLett.107.011802.
- [67] P. Astier, et al., Search for $\nu_\mu \rightarrow \nu_e$ oscillations in the NOMAD experiment, Phys. Lett. B570 (2003) 19–31. arXiv:hep-ex/0306037, doi:10.1016/j.physletb.2003.07.029.
- [68] B. Armbruster, et al., Upper limits for neutrino oscillations muon-anti-neutrino \rightarrow electron-anti-neutrino from muon decay at rest, Phys. Rev. D65 (2002) 112001. arXiv:hep-ex/0203021, doi:10.1103/PhysRevD.65.112001.
- [69] M. Antonello, et al., Experimental search for the LSND anomaly with the ICARUS detector in the CNGS neutrino beam, Eur. Phys. J. C73 (3) (2013) 2345. arXiv:1209.0122, doi:10.1140/epjc/s10052-013-2345-6.
- [70] L. Borodovsky, et al., Search for muon-neutrino oscillations muon-neutrino \rightarrow electron-neutrino (anti-muon-neutrino \rightarrow anti-electron-neutrino) in a wide band neutrino beam, Phys. Rev. Lett. 68 (1992) 274–277. doi:10.1103/PhysRevLett.68.274.
- [71] M. Maltoni, T. Schwetz, Testing the statistical compatibility of independent data sets, Phys. Rev. D68 (2003) 033020. arXiv:hep-ph/0304176, doi:10.1103/PhysRevD.68.033020.
- [72] G. Karagiorgi, A. Aguilar-Arevalo, J. M. Conrad, M. H. Shaevitz, K. Whisnant, M. Sorel, V. Barger, Leptonic CP violation studies at MiniBooNE in the (3+2) sterile neutrino oscillation hypothesis, Phys. Rev. D75 (2007) 013011, [Erratum: Phys. Rev. D80,099902(2009)]. arXiv:hep-ph/0609177, doi:10.1103/PhysRevD.75.013011, 10.1103/PhysRevD.80.099902.
- [73] M. Maltoni, T. Schwetz, Sterile neutrino oscillations after first MiniBooNE results, Phys. Rev. D76 (2007) 093005. arXiv:0705.0107, doi:10.1103/PhysRevD.76.093005.
- [74] P. A. R. Ade, et al., Planck 2015 results. XIII. Cosmological parameters arXiv:1502.01589.
- [75] J. Bergström, M. C. Gonzalez-Garcia, V. Niro, J. Salvado, Statistical tests of sterile neutrinos using cosmology and short-baseline data, JHEP 10 (2014) 104. arXiv:1407.3806, doi:10.1007/JHEP10(2014)104.
- [76] H. Nunokawa, O. L. G. Peres, R. Zukanovich Funchal, Probing the LSND mass scale and four neutrino scenarios with a neutrino telescope, Phys. Lett. B562 (2003) 279–290. arXiv:hep-ph/0302039, doi:10.1016/S0370-2693(03)00603-8.
- [77] B. J. P. Jones, Sterile Neutrinos in Cold Climates, ph.D. thesis, Massachusetts Institute of Technology, 2015.
- [78] Argüelles Delgado, C. A., New Physics with Atmospheric Neutrinos, ph.D. thesis, University of Wisconsin-Madison, 2015.
- [79] M. C. Gonzalez-Garcia, M. Maltoni, Determination of matter potential from global analysis of neutrino oscillation data, JHEP 09 (2013) 152. arXiv:1307.3092, doi:10.1007/JHEP09(2013)152.
- [80] L. Wolfenstein, Neutrino Oscillations in Matter, Phys. Rev. D17 (1978) 2369–2374. doi:10.1103/PhysRevD.17.2369.
- [81] S. P. Mikheev, A. Yu. Smirnov, Resonance Amplification of Oscillations in Matter and Spectroscopy of Solar Neutrinos, Sov. J. Nucl. Phys. 42 (1985) 913–917, [Yad. Fiz.42,1441(1985)].
- [82] O. G. Miranda, M. A. Tortola, J. W. F. Valle, Are solar neutrino oscillations robust?, JHEP 10 (2006) 008. arXiv:hep-ph/0406280, doi:10.1088/1126-6708/2006/10/008.
- [83] S. Davidson, C. Pena-Garay, N. Rius, A. Santamaria, Present and future bounds on nonstandard neutrino interactions, JHEP 03 (2003) 011. arXiv:hep-ph/0302093, doi:10.1088/1126-6708/2003/03/011.
- [84] C. Biggio, M. Blennow, E. Fernandez-Martinez, General bounds on non-standard neutrino interactions, JHEP 08 (2009) 090. arXiv:0907.0097, doi:10.1088/1126-6708/2009/08/090.

- [85] M. B. Gavela, D. Hernandez, T. Ota, W. Winter, Large gauge invariant non-standard neutrino interactions, *Phys. Rev. D* 79 (2009) 013007. [arXiv:0809.3451](https://arxiv.org/abs/0809.3451), [doi:10.1103/PhysRevD.79.013007](https://doi.org/10.1103/PhysRevD.79.013007).